The dynamic ocean biological pump: Insights from a global compilation of particulate organic carbon, $CaCO_3$, and opal concentration profiles from the mesopelagic

Phoebe J. Lam,[1] Scott C. Doney,[1] and James K. B. Bishop[2]

Received 15 May 2010; revised 17 February 2011; accepted 4 April 2011; published 22 July 2011.

[1] We have compiled a global data set of 62 open ocean profiles of particulate organic carbon (POC), $CaCO_3$, and opal concentrations collected by large volume in situ filtration in the upper 1000 m over the last 30 years. We define concentration-based metrics for the strength (POC concentration at depth) and efficiency (attenuation of POC with depth in the mesopelagic) of the biological pump. We show that the strength and efficiency of the biological pump are dynamic and are characterized by a regime of constant and high transfer efficiency at low to moderate surface POC and a bloom regime where the height of the bloom is characterized by a weak deep biological pump and low transfer efficiency. The variability in POC attenuation length scale manifests in a clear decoupling between the strength of the shallow biological pump (e.g., POC at the export depth) and the strength of the deep biological pump (POC at 500 m). We suggest that the paradigm of diatom-driven export production is driven by a too restrictive perspective on upper mesopelagic dynamics. Indeed, our full mesopelagic analysis suggests that large, blooming diatoms have low transfer efficiency and thus may not export substantially to depth; rather, our analysis suggests that ecosystems characterized by smaller cells and moderately high $\%CaCO_3$ have a high mesopelagic transfer efficiency and can have higher POC concentrations in the deep mesopelagic even with relatively low surface or near-surface POC. This has negative implications for the carbon sequestration prospects of deliberate iron fertilization.

Citation: Lam, P. J., S. C. Doney, and J. K. B. Bishop (2011), The dynamic ocean biological pump: Insights from a global compilation of particulate organic carbon, $CaCO_3$, and opal concentration profiles from the mesopelagic, *Global Biogeochem. Cycles*, *25*, GB3009, doi:10.1029/2010GB003868.

1. Introduction

[2] The biological carbon pump in the ocean lowers atmospheric CO_2 by transferring carbon from the surface ocean to deeper waters via sinking particulate organic carbon (POC). Both the strength (magnitude) and the efficiency (remineralization length scale) of the transfer of POC to depth are important for atmospheric CO_2 [*Kwon et al.*, 2009; *Marinov et al.*, 2006; *Matsumoto et al.*, 2007; *Volk and Hoffert*, 1985].

[3] Efforts to understand the factors controlling the strength and magnitude of POC flux to depth generally focus on understanding food web processes or on the potential role of ballast minerals [*Boyd and Trull*, 2007]. The "ballast hypothesis" grew out of observed correlations in deep (>1000 m) sediments traps between POC flux and the flux of ballast minerals ($CaCO_3$, opal and dust) in the Equatorial Pacific [*Armstrong et al.*, 2002]. Global compilations of deep sediment trap data further revealed a tighter correlation between either strength or efficiency of POC flux and $CaCO_3$ flux compared with opal or dust flux [*François et al.*, 2002; *Klaas and Archer*, 2002]. Recently, investigators also observed a better correlation between $CaCO_3$ and POC shallow export flux at the base of the mixed layer in samples taken along the Atlantic Meridional Transect and in the subpolar North Atlantic [*Sanders et al.*, 2010], suggesting that the ballast relationship may be set high in the water column. Whether there is a mechanistic basis underlying the ballast relationship is still in dispute, however [*Boyd and Trull*, 2007].

[4] The biggest gradient in POC flux occurs in the mesopelagic zone, the region between the base of the euphotic zone and about 1000 m. Because of difficulties in sampling POC flux in the mesopelagic zone [*Buesseler et al.*, 2007a], the global coverage of POC flux data is best for shallow export flux, where other methods such as the ^{234}Th-^{238}U disequilibrium method can be used [*Buesseler*, 1998; *Buesseler and Boyd*, 2009], and in the bathypelagic (>1500 m), where bottom-moored sediment traps are reliable collectors of sinking particles [*Yu et al.*, 2001] and have been used successfully for almost three decades [*François et al.*,

[1]Department of Marine Chemistry and Geochemistry, Woods Hole Oceanographic Institution, Woods Hole, Massachusetts, USA.
[2]Department of Earth and Planetary Science, University of California, Berkeley, California, USA.

0886-6236/11/2010GB003868

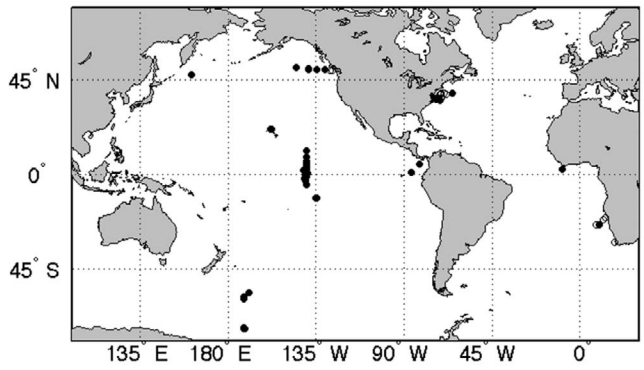

Figure 1. Locations of 75 open ocean profiles (MU)LVFS profiles collected from 1976 to 2005. Stations with closed symbols (N = 62) are open ocean stations used in the analysis.

2002; *Honjo et al.*, 2008; *Klaas and Archer*, 2002; *Lutz et al.*, 2002].

[5] Corrections for trapping efficiency and ongoing improvements in sediment trap design are allowing continuing additions to the mesopelagic flux database. Early compilations suggest large geographic and temporal variability in the attenuation of POC in the mesopelagic [*Buesseler et al.*, 2007b; *Lee et al.*, 2009; *Lomas et al.*, 2010; *Lutz et al.*, 2002]. This is in contrast to what was predicted by the Open Ocean Composite from the VERTEX mesopelagic flux studies in the 1980s in the North Pacific [*Martin et al.*, 1987]. The need for better spatial and temporal data density requires additional and complementary tools for studying the sedimentation of POC in the mesopelagic.

[6] POC concentration profiles are a good complement to POC flux profiles for understanding the functioning of the ocean biological pump, since these are conceptually linked by particle sinking speed (flux = sinking speed * concentration). Further, the standing stock of POC is the source of fixed carbon for consumers, so its time and space variability is an important determinant of the mesopelagic ecosystem. Finally, POC concentration profiles are easier to measure than flux profiles, and can thus provide increased vertical, geographic and temporal data density.

[7] Compared to POC flux studies, there has been relatively little attention paid to the distribution of POC concentration profiles in the mesopelagic. A global data set of particle size distribution and abundance from camera-based imaging techniques was recently compiled and converted to mass flux using simple power law relationships to relate particle size spectrum to mass flux [*Guidi et al.*, 2008, 2009]. While camera-based profiles are very impressive in their resolution and ability to distinguish particle size spectra, they ultimately do not provide direct geochemical information, and require that certain assumptions be made to extract mass and POC content.

[8] Traditional methods to collect particles allow for direct analysis of POC, and further permit other geochemical analyses such as of biogenic ballast minerals. While particle size spectra are much more difficult to determine on particles on a filter, methods such as large volume in situ pumping can nonetheless provide some size-fractionated concentration data, allowing separation of the sinking and suspended size fractions.

[9] Here we compile and analyze the sinking size fraction (>53 μm) of 62 open ocean concentration profiles of POC, $CaCO_3$, and opal collected by large volume in situ filtration in the upper 1000 m over the last 30 years. Our strategy is to analyze the compiled concentration profile data directly rather than converting them to fluxes to avoid potential model-dependent errors. In section 2.4, we define concentration-based metrics for the strength and efficiency of the biological pump that are analogous to traditional flux-based definitions of the biological pump. Our concentration-based metrics are analogous to but not equivalent to the traditional flux-based definitions of the biological pump. They are fully self-consistent and thus provide a complementary view of the global distribution of the strength and efficiency of POC transport to depth, and the role of biogenic ballast minerals.

2. Methods

2.1. Description of (MU)LVFS Archive

[10] The Multiple Unit Large Volume in situ Filtration System (MULVFS) [*Bishop et al.*, 1985] and precursor systems have been used for over 30 years to collect more than 70 profiles of size-fractionated (>53 μm, 1–53 μm, <1 μm) suspended particle data from the surface and mesopelagic ocean (ca. 100 to 1000 m) from a wide geographical range (Figure 1 and Table 1) [*Bishop*, 1992, 1999; *Bishop et al.*, 1999, 1980, 1977; *Bishop and Fleisher*, 1987; *Bishop et al.*, 1978, 1986; *Bishop and Wood*, 2008; *Lam and Bishop*, 2007].

[11] The MULVFS data set offers several advantages over sediment traps deployed in the mesopelagic: MULVFS profiles have up to 12 samples between the surface and 1000 m, compared to a more typical 3–5-depth profile from mesopelagic traps (*Buesseler et al.* [2007b], *Martin et al.* [1987], Bermuda Atlantic Time Series Study, available at http://bats.bios.edu, and Hawaii Ocean Time series Data Organization and Graphical System, available at http://hahana.soest.hawaii.edu/hot/hot-dogs/interface.html); the samples are not subject to collection problems that can plague sediment traps in the mesopelagic [*Buesseler et al.*, 2007a]; and all samples were collected by a single investigator with self-consistent sampling and handling protocols [*Bishop et al.*, 1985; *Bishop and Wood*, 2008]. The MULVFS archive further offers some midlatitude seasonal coverage (line P in the eastern subarctic Pacific) that is generally unavailable for mesopelagic POC flux.

[12] POC concentrations can be converted to fluxes by multiplying by particle sinking speed, and taking into account variations in particle composition, shape, and size spectra [*Bishop et al.*, 1986; *Guidi et al.*, 2008; *Stemmann et al.*, 2004]. These parameters were carefully assessed chemically and microscopically in MULVFS profiles from the Panama Basin in order to convert POC concentrations to POC flux [*Bishop et al.*, 1986]. However, this process is extremely labor intensive and these parameters were not routinely evaluated for the rest of the MULVFS data set. As a result, and to avoid model-dependent errors in converting from concentration to flux, here we focus on the >53 μm concentration data directly, which is the putative sinking size class.

2.2. Major Particulate Phases Determination

[13] Most of the particulate composition data compiled here is already published or in online databases (see

Table 1. Profile Number, Descriptions, Locations, Times of Collection, Euphotic Zone Depths (z_{eu}), Mixed Layer Depths (MLD), Reference Depths (z_0), and References for All Open Ocean Profiles Used in This Compilation

	Description	Lat (deg)	Long (deg)	Date (mm/dd/yy)	z_{eu} (m)	MLD (m)	z_0 (m)	References and Notes[a]
				Other				
1	Eq. Atl.	2.8	−8.9	12/19/73	80	40	80	1[b]
2	Cape Basin	−25.2	10.0	01/01/73	80	50	80	2[b]
3	Cape Basin	−25.4	8.0	01/05/73	80	65	90	2[b,c]
4	Panama Basin	0.8	−86.2	07/02/76	70	30	70	3[d]
5	Panama Basin	5.0	−82.0	08/02/79	70	18	70	4[e]
6	Panama Basin	5.0	−82.0	11/23/79	70	35	70	4[e]
				Warm Core Rings (WCR)				
7	WCR Apr82 core	38.9	−71.3	04/22/82	80	400	400	5[c]
8	WCR Jun82 core	36.7	−73.8	06/24/82	60	40	60	5[f,g]
9	WCR Aug82core	36.9	−73.7	08/12/82	150	150	150	5[f,g]
11	WCR Gulf Stream	37.1	−70.9	08/21/82	150	150	150	5[f,g,h]
12	WCR Oct82 core	39.5	−65.4	10/07/82	60	80	80	5[b,f]
				Eastern Subarctic Pacific: Line P				
13	OSP Feb96	50.0	−145.0	03/01/96	80	100	100	6[i,j]
14	P16 May96	49.3	−134.7	05/13/96	40	105	105	6[i,j]
15	P20 May96	49.6	−138.7	05/16/96	35	65	65	6[i,j]
16	OSP May96n	50.0	−145.0	05/19/96	60	95	95	6[i,j]
17	OSP May96d	50.0	−145.0	05/21/96	60	95	95	6[c]
18	P12 May96	49.0	−130.7	05/26/96	60	80	80	6[i,j]
19	P12 Aug96	49.0	−130.7	08/19/96	40	20	40	6[i,j]
20	P16 Aug96	49.3	−134.7	08/22/96	40	25	40	6[i,j]
21	P20 Aug96	49.3	−138.7	08/25/96	35	25	35	6[i,j]
22	OSP Aug96n	50.0	−145.0	08/29/96	40	15	40	6[i,j]
23	P12 Feb97avg	49.0	−130.7	02/25/97	60	105	105	6[i,j,k]
24	P16 Feb97	49.3	−134.7	02/16/97	60	95	95	6[i,j]
				Subantarctic Pacific: SOFeX–55°S				
25	55°S1−Fe	−56.5	−172.0	01/12/02	90	40	90	7[l]
26	55°S2 +Fe	−55.8	−171.9	01/19/02	90	50	90	7[l]
32	55°S8 +Fe	−54.2	−169.3	02/09/02	60	30	60	7[l]
				Antarctic Pacific: SOFeX–66°S				
27	66°S3 −Fe	−66.4	−171.5	01/23/02	60	45	60	7[l]
28	66°S4 +Fe	−66.4	−171.9	01/27/02	60	45	60	7[c,l]
29	66°S5 +Fe	−66.4	−171.5	01/31/02	45	45	45	7[l]
30	66°S6 −Fe	−66.4	−171.7	02/02/02	60	45	60	7[l]
31	66°S7 +Fe	−66.2	−172.0	02/04/02	45	45	45	7[l]
				Oligotrophic				
10	WCR Sargasso	36.0	−71.5	08/19/82	120	120	120	5[f,g]
33	ALOHA 1d	22.7	−158.0	06/25/04	125	49	125	8[e]
34	ALOHA 2n	22.7	−158.1	06/26/04	125	49	125	8[e]
35	ALOHA 4n	22.8	−158.0	07/05/04	125	49	125	8[e]
				Western Subarctic Pacific: Station K2				
36	K2 M7d	47.0	161.0	07/31/05	50	26	50	8[e]
37	K2 M8n	47.0	161.0	08/01/05	50	26	50	8[e]
38	K2 M9d	47.1	161.0	08/11/05	50	26	50	8[e]
39	K2 M10n	47.1	161.0	08/12/05	50	26	50	8[e]
				JGOFS Equatorial Pacific Survey 1				
40	EqPac 9N1	9.0	−140.0	02/08/92	109	67	109	9,10[m]
41	EqPac 5N1	5.2	−139.9	02/13/92	116	86	116	9,10[m]
42	EqPac 3N1	3.0	−140.0	02/15/92	118	110	118	9,10[m]
43	EqPac 2N1	2.1	−140.0	02/18/92	120	66	120	9,10[m]
44	EqPac 1N1	1.4	−140.5	02/21/92	124	99	124	9,10[m]
45	EqPac EQ1	0.0	−140.4	02/24/92	140	44	140	9,10[m]
46	EqPac 1S1	−1.1	−140.3	02/27/92	116	51	116	9,10[m]
47	EqPac 2S1	−2.0	−140.8	03/01/92	140	83	140	9,10[m]
48	EqPac 5S1	−5.1	−140.0	03/03/92	124	79	124	9,10[m]
49	EqPac 12S1	−12.0	−135.0	03/07/92	136	53	136	9,10[m]
				JGOFS Equatorial Pacific Survey 2				
50	EqPac 12N2	12.0	−140.1	08/11/92	120	52	120	9,10[n]
51	EqPac 9N2	9.0	−140.0	08/13/92	114	51	114	9,10[h,n]
52	EqPac 7N2	7.0	−139.9	08/17/92	122	78	122	9,10[n]
53	EqPac 5N2	5.0	−139.8	08/20/92	112	51	112	9,10[n]

Table 1. (continued)

	Description	Lat (deg)	Long (deg)	Date (mm/dd/yy)	z_{eu} (m)	MLD (m)	z_0 (m)	References and Notes[a]
54	EqPac 3N2	2.8	−140.4	08/22/92	100	57	100	9,10[n]
55	EqPac 2N2	2.1	−141.3	08/26/92	98	16	98	9,10[n]
56	EqPac 1N2	1.3	−140.0	08/27/92	92	10	92	9,10[n]
57	EqPac EQ2	0.3	−139.6	08/30/92	92	47	92	9,10[n]
58	EqPac 1S2	−1.1	−140.0	09/01/92	118	58	118	9,10[n]
59	EqPac 2S2	−2.4	−140.5	09/04/92	98	72	98	9,10[n]
60	EqPac 3S2	−3.4	−140.5	09/06/92	108	50	108	9,10[n]
61	EqPac 5S2	−5.4	−139.8	09/09/92	98	79	98	9,10[n]
62	EqPac 12S2	−11.9	−135.0	09/14/92	138	70	138	9,10[n]

[a]References: 1, *Bishop et al.* [1977]; 2, *Bishop et al.* [1978]; 3, *Bishop et al.* [1980]; 4, *Bishop et al.* [1986]; 5, *Bishop and Fleisher* [1987]; 6, *Bishop et al.* [1999]; 7, *Lam and Bishop* [2007]; 8, *Bishop and Wood* [2008]; 9, *Bishop* [1992]; 10, *Bishop* [1999].
[b]The z_{eu} from MODIS.
[c]Too few data points to fit.
[d]Known particle loss.
[e]The z_{eu} reported in primary reference.
[f]Less than 53 μm POC is 1–53 μm only.
[g]The z_{eu} estimated from vertical chlorophyll sections by *Smith and Baker* [1985].
[h]Bad fit.
[i]MLD is 1st depth where $\Delta\sigma_\theta > 0.05$.
[j]The z_{eu} from *Sherry et al.* [1999].
[k]Average of day and night profiles.
[l]The z_{eu} is estimated from beam attenuation profiles by *Bishop et al.* [2004].
[m]The z_{eu} is estimated as 1% of surface downwelled 486 nm irradiance from *Trees* [1992a].
[n]The z_{eu} is estimated as 1% of surface downwelled nm irradiance from *Trees* [1992b].

references in Table 1), but we have recalculated some quantities. The >53 μm particulate organic matter (POM) of a majority of the profiles in this data set (59/75) was estimated gravimetrically as the difference between salt-corrected dry weight and the stoichiometric masses of major phases determined chemically ($CaCO_3$, opal, $SrSO_4$, where applicable). Lithogenic mass was generally not measured. Since lithogenics could be a significant portion of suspended particulate mass, particularly near coastal margins, it would be included as an artifact in the gravimetric POC estimate. We thus exclude all profiles collected from coastal margins (<3000 m water depth), reducing the data set to 62 profiles. Focusing only on profiles from open ocean regions also minimizes lateral influences that would violate our one-dimensional assumption in the power law fits described below. The references, locations and times of collections for these 62 profiles are reported in Table 1.

[14] Most of the original papers used a simple organic matter composition of CH_2O (POM:POC = 2.5) to scale gravimetric POM to POC; here we recalculated POC using an updated POM:POC = 1.88 that is consistent with inverse [*Anderson*, 1995; *Anderson and Sarmiento*, 1994] and NMR [*Hedges et al.*, 2002] determinations of the organic matter composition [cf. *Lam and Bishop*, 2007; *Timothy et al.*, 2003]. Exceptions to gravimetric determination of POC are noted as follows.

[15] Deep gravimetric POC data from SOFeX (profiles 25–32; see Table 1) were noisy and inconsistent with several other proxies of organic matter determination, so POC was estimated using a combination of particulate phosphorus, directly determined C:P of the small size fraction, and gravimetric POC at the surface ("POCPscale") [*Lam and Bishop*, 2007]. For a few of the profiles, >53 μm particles were scraped (profile 1) or rinsed (profiles 33–39) off the prefilter screens and the POC was determined directly by combustion. We unfortunately do not have direct comparisons between the gravimetric and direct combustion methods, but POC profiles from similar biomes analyzed using the two methods compare well. The oligotrophic North Pacific ALOHA POC profiles from the direct combustion after rinsing method are similar in magnitude and shape to the oligotrophic North Atlantic Sargasso Sea POC profile from the gravimetric method; similarly, the K2 (western subarctic Pacific) POC profiles from the direct combustion method compares well to POC profiles from the eastern subarctic Pacific determined gravimetrically, and are clearly different than the oligotrophic profiles, suggesting that there is consistency between methods.

[16] $CaCO_3$ and opal concentrations were taken directly from the papers, with $CaCO_3$ determined stoichiometrically from sea salt corrected Ca, and opal determined spectrophotometrically after a weak base (1.0N NaOH or 0.4M Na_2CO_3) leach. $CaCO_3$ and opal data from the JGOFS EqPac project are reported here for the first time.

[17] We also report <53 μm POC from the original papers as the sum of <1 μm and 1–53 μm POC determined directly by combustion of samples collected on the bottom and top filters of precombusted paired quartz fiber filters, respectively. We do not report $CaCO_3$ or opal from the <53 μm size fraction, because this data was not available for the entire data set. Total POC is the sum of <53 μm and >53 μm POC. Compiled <53 μm POC, >53 μm POC, $CaCO_3$, and opal concentrations are presented in Data Set S1.[1]

2.3. The 1-D Modeling of POC Profiles

[18] Like with POC flux to depth, POC concentration profiles in the mesopelagic zone are empirically well fit with a power law function. Here, we fit the open ocean >53 μm POC concentration profiles with a power law:

$$P(z) = P_0 \left(\frac{z}{z_0}\right)^{-b} \quad (1)$$

[1]Auxiliary material data sets are available at ftp://ftp.agu.org/apend/journal/2010GB003868. Other auxiliary material files are in the HTML.

where $P(z)$ is the fitted POC concentration at depth z, b is the power law exponent, and P_0 is the initial POC concentration at the reference depth z_0 [*Lam and Bishop*, 2007].

[19] While there are physical motivations for the power law fit (see Text S1), here we use it as an empirical tool to interpolate between data points and as a convenient way to assess the differences in the magnitudes and shapes of the >53 μm POC profiles using the parameters from the fit (P_0 and b value) as metrics for the strength and efficiency of the biological pump.

[20] The values of the power law parameters P_0 and b value are very sensitive to the choice of z_0. The 1-D power law model is only valid below the zone of particle production, where sinking and remineralization are the only important processes (Text S1). We make the assumption that particle production will occur throughout the euphotic zone, but if the mixed layer depth (MLD) is deeper than the euphotic zone depth (z_{eu}), newly produced particles will be mixed throughout the MLD. We thus define the reference depth z_0 for each profile as the deeper of the MLD and z_{eu}. MLDs and z_{eu} were taken from the original references or from other papers published from the same cruise when possible (Table 1). When not reported in the literature, we estimated z_{eu} using the appropriate month's climatology of the MODIS euphotic zone depth data product [*Lee et al.*, 2007]. The euphotic zone depth was as deep or deeper than the MLD, and thus taken as the reference depth, z_0, for all profiles except for a subset of the CJGOFS Line P profiles from the eastern subarctic Pacific. For the Line P profiles, the MLD was defined as the first depth where the change in potential density from the surface was greater than 0.05 kg/m^3, a criterion characteristic of diurnal mixing [*Bishop and Wood*, 2009].

[21] Profiles were fit using linear regressions to log-transformed depth and POC data below the reference depth, z_0 (fitted slope and intercept are b and P_0, respectively). This method of fitting better captured deep POC data than non-linear fitting routines. Data points below z_0 that were clear outliers and did not decrease monotonically with depth were flagged and not included in the regressions. Of the 62 open ocean profiles, 55 profiles were well fit with a power law, with the poor fits due mostly to insufficient data points (Table 1). Total POC was also fit with a power law function using z_0 as defined above for interpolation purposes only.

2.4. Metrics for Assessing Strength and Efficiency of Biological Pump

[22] As metrics for euphotic zone biomass, we report the maximum >53 μm POC (*maxPOC*) and maximum total POC (*maxtPOC*) concentrations for each profile. Note that *maxPOC* and *maxtPOC* are not always at the same depth. These metrics may easily underestimate the true POC maximum if the pump was not positioned precisely at the depth of the true maximum. In this paper, we assume a fixed 25% relative uncertainty for measured euphotic zone POC values to account for observed diurnal variability in euphotic zone POC of ~25% in both oligotrophic and mesotrophic environments [*Bishop and Wood*, 2008], and uncertainties in individual measurements of 2–40% based on repeat profiles at a single location.

[23] The fitted POC concentration at the reference depth, P_0, can be thought of as the POC concentration poised to sink into the mesopelagic zone. While the value of P_0 is model-dependent and sensitive to the choice of z_0, it circumvents the sampling bias associated with *maxPOC*. Here we use P_0 as a metric for the magnitude or "strength" of the shallow biological pump, analogous to export production.

[24] The power law exponent, b, describes how quickly P_0 is attenuated with depth, and scales with the ratio between particle remineralization rate and sinking speed (Text S1). Larger values of b from faster remineralization rates and/or slower sinking speeds indicate more rapid attenuation of POC with depth and thus a lower "efficiency" for the biological pump.

[25] As a metric for the "strength" of the deep biological pump, we report the >53 μm and total POC concentrations at 500 m (P_{500} and tP_{500}) from power law fits to mesopelagic POC concentration, and also P_{0+500}, the magnitude of the fitted POC concentration at z_{0+500}, 500 m below z_0. The fitted values for P_{500} and P_{0+500} are insensitive or only weakly sensitive to choice of z_0, and can be used as a model independent interpolation between data points. Finally, we define a mesopelagic transfer efficiency, TE_{P0+500}, analogous to the one often defined for particle flux [*Buesseler and Boyd*, 2009; *François et al.*, 2002; *Lomas et al.*, 2010]:

$$TE_{P0+500} = P_{0+500}/P_0 \quad (2)$$

A higher transfer efficiency indicates a smaller attenuation of POC with depth (smaller b value) and a longer remineralization length scale.

[26] It is important to note that the concentration-based metrics for the strength and efficiency of the biological pump defined here are analogous to but not equivalent to the traditional flux-based metrics. We nonetheless use the same terminology to emphasize the parallels.

[27] Uncertainties in the metrics of the strength and efficiency of the biological pump are the uncertainties in the fit parameters in the case of P_0 and b, and the regression uncertainty for P_{500} and P_{0+500}. Fit parameters and their 95% confidence intervals (95% CI) are reported in Data Set S2. Errors are plotted as standard errors, which are the 95% CI divided by the appropriate critical t statistic for the degrees of freedom in the fit.

3. Results and Discussion

3.1. Description of Euphotic Zone >53 μm Particle Types in the Data Set

[28] The >53 μm particles in the data set comprises a wide variety of particle types, with euphotic zone $CaCO_3$ and POC concentrations ranging over an order of magnitude from 0 to 17 μg/kg and 2 to 95 μg/kg, respectively, and opal concentrations ranging more than 2 orders of magnitude, from 0.2 to 121 μg/kg. The weight fractions of major particulate phases in the >53 μm fraction in the euphotic zone ranged from 0—34% $CaCO_3$, 4–73% opal, and 21–90% particulate organic matter (Figure S2). The contribution to total POC from the >53 μm size fraction (f_{large}) ranges from regions where most of the total euphotic zone POC is in the large >53 μm size fraction (f_{large} = 0.8 in the Southeast Atlantic at the edge of the Benguela Upwelling Zone), to those where the large particles are a small fraction of total POC (f_{large} = 0.1 at 12°S during EqPac). Regions dominated

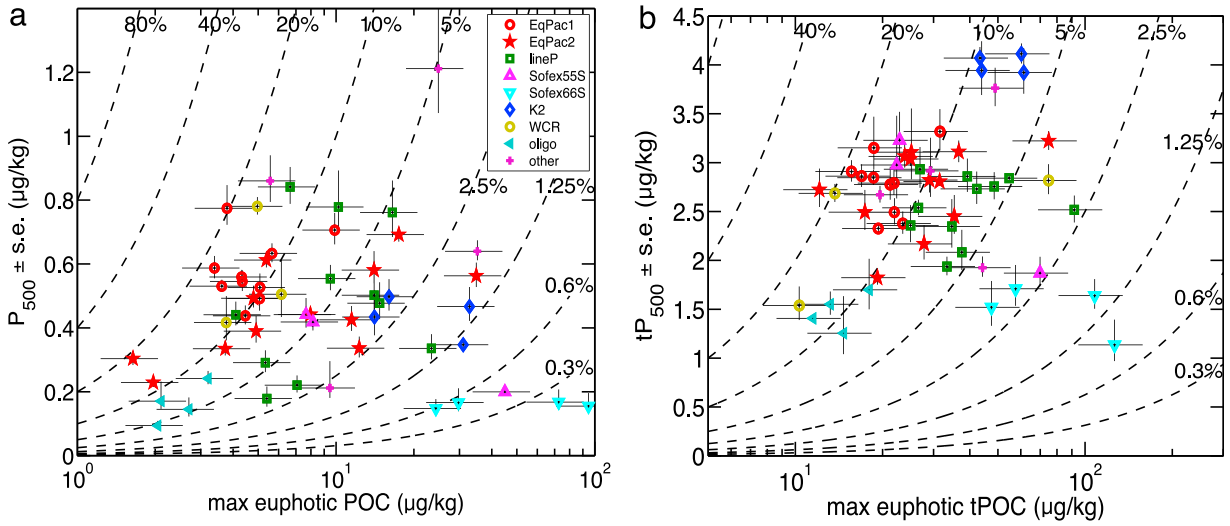

Figure 2. Relationship between maximum euphotic POC and P_{500}, the fitted POC concentration at 500 m for (a) >53 μm fraction and (b) total POC. Dashed curves are lines of constant transfer efficiency of POC between the depth of maximum POC (maxPOC) and 500 m (P500) for >53 μm POC (Figure 2a) and total POC (Figure 2b). Stations are assigned symbols according to biogeographical groupings (Table 1). Error bars for P_{500} are standard errors of the fit and are a fixed 25% relative standard deviation for maximum euphotic POC. Note the log scale on the *x* axis.

by large cells (f_{large} > 0.5) were restricted to regions with a low weight fraction of $CaCO_3$ (f_{CaCO3} < 0.06) (Figure S1).

3.2. Distribution and Variability in POC Profile Shapes

[29] Maximum >53 μm POC concentrations in the euphotic zone (*maxPOC*) range almost two orders of magnitude (Data Set S1). The lowest values (~1–3 μg/kg) are toward the gyres at 7°N and 12°S during Equatorial Pacific Survey 2 and at the oligotrophic sites. The highest values (~40–95 μg/kg) are at the Southern Ocean Iron Experiment (SOFeX) sites after deliberate iron fertilization.

[30] Whereas *maxPOC* ranged over two orders of magnitude, POC concentrations at 500 m (P_{500}) show a reduced range of only 1 order of magnitude, from a minimum of 0.09 (95%CI = 0.07 to 0.13) μg/kg at the ALOHA station in the subtropical North Pacific to a maximum of 1.2 (0.9 to 1.7) μg/kg in the Panama Basin (Data Set S1). The ALOHA station had one of the lowest POC concentrations in the euphotic zone (*maxPOC* = 2.05 μg/kg) and it is thus not surprising that it also had the lowest POC concentration at 500 m (P_{500} = 0.094 μg/kg) (Data Set S1 and Figure 2a). Surprisingly, the blooming Antarctic stations, which had the highest euphotic zone POC (*maxPOC* > 70 μg/kg), also had among the lowest P_{500} (P_{500} < 0.17 μg/kg). The highest POC concentrations at 500 m were found at stations with moderate euphotic zone POC (Figure 2a).

[31] The transfer efficiency of euphotic zone POC to 500 m ranged from 0.2 to 20%, with an average of 7%. Although there is scatter in the relationship, there is a clear decrease in the transfer efficiency of euphotic zone POC to 500 m with increasing *maxPOC*, and an indication of decreasing P_{500} with increasing *maxPOC* at moderate to high *maxPOC* (Figure 2a). Similar trends can also be seen in total POC, with the decreasing trend in total POC at 500 m (tP_{500}) with increasing total euphotic zone biomass (*maxtPOC*) even more apparent (Figure 2b).

3.3. Distribution and Variability in Biological Pump Metrics

[32] Because of the likely sampling bias associated with the *maxPOC* metric, we also use P_0, the fitted >53 μm POC concentration at the reference depth, as an alternative indicator of near surface POC. Globally, *maxPOC* and P_0 are correlated, with P_0 representing 17% of the *maxPOC* on average (Figure 3).

[33] When P_0 is plotted against the fitted >53 μm POC concentration 500 m below the reference depth, P_{0+500}, the same general pattern can be seen as with the raw data: the

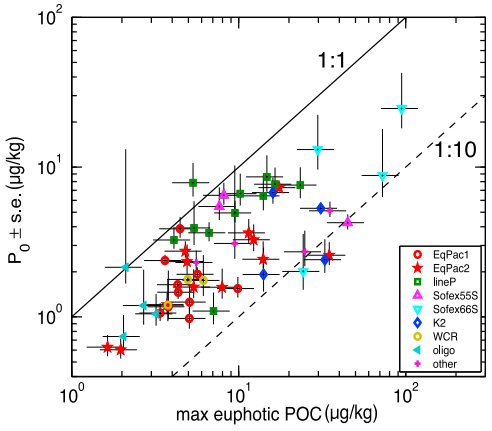

Figure 3. Relationship between >53 μm maximum euphotic POC and P_0, the fitted >53 μm POC concentration at the reference depth. The 1:1 and 1:10 lines are plotted as solid and dashed black lines, respectively. Error bars as for Figure 2.

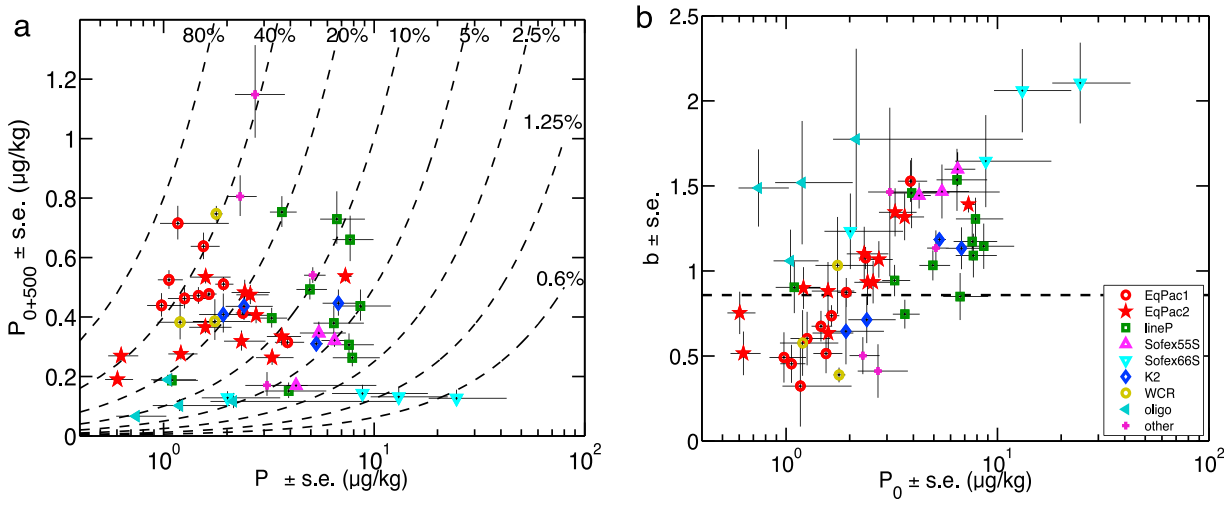

Figure 4. Relationship between P_0 and the (a) strength (P_{0+500}, the >53 μm POC concentration 500 m below the reference depth) and (b) efficiency (b, the power law exponent) of the biological pump. Dashed curves in Figure 4a are lines of constant mesopelagic transfer efficiency of POC between the reference depth and 500 m below (TE_{P0+500}). Dashed horizontal line in Figure 4b is canonical Martin Open Ocean Composite b = 0.858. Error bars are standard errors of the fit. Note the log scale on the x axis.

lowest P_{0+500} is at the lower and upper extremes of P_0, and there is a general decreasing trend in both P_{0+500} and in mesopelagic transfer efficiency, TE_{P0+500}, as P_0 increases from moderate to high values (Figure 4a). The highest P_{0+500} and TE_{P0+500} are at moderate P_0. For example, the station with the highest P_{0+500} (P_{0+500} = 1.1 μg/kg in the Panama Basin) had only a moderate P_0 (P_0 = 2.7 μg/kg), and one of the higher mesopelagic transfer efficiencies (TE_{P0+500} = 42%) in the data set.

[34] The decrease in the efficiency of the biological pump with increasing P_0 can also be seen in the power law exponent, with a trend to increasing b value (increasing attenuation) with increasing P_0 (Figure 4b). The observed variability in the vertical attenuation length scale of POC as evidenced by widely ranging TE_{P0+500} and b values is in contrast to the fixed b value of 0.858 and an equivalent TE_{P0+500} = 21% given by *Martin et al.*'s [1987] Open Ocean Composite of POC flux.

[35] Attenuation of POC was highest at the Antarctic station following iron addition, with a b value of 2.1 (95%CI = 1.52 to 2.69) (Data Set S1). The strong attenuation (high b value) and low mesopelagic transfer efficiency that characterized the blooming Antarctic stations were more important for determining P_{0+500} than their higher surface or near surface POC starting points (Figure 4a). Factors determining variability in mesopelagic transfer efficiency are at least as important as (and sometimes more important than) the magnitude of the starting material concentration.

[36] A positive trend between flux at 100 m (analogous to P_0) and b value was also observed in compilations of U.S. JGOFS POC flux profiles [*Berelson*, 2001]. Uncertainties in measured mesopelagic fluxes and thus in the fit parameters were high, however, and may have led to a spurious correlation because of a statistical artifact [*Primeau*, 2006]. In the MULVFS data set, collection problems are not as important, and the much higher vertical resolution, particularly in the upper mesopelagic, results in better constrained fit parameters and thus trend between P_0 and b value. Nonetheless, the relationship between P_0 and b value can be viewed simply as a representation of the fact that the dynamic range in POC is much higher in the euphotic zone than at 500 m. This is an interesting observation, suggesting that there is a mechanism that keeps excess POC produced at the surface from propagating down the water column.

3.4. The Dynamic Biological Pump: Changing Strength and Efficiency

[37] The same general pattern of elevated deep mesopelagic POC concentrations at moderate surface or near-surface POC concentrations flanked by low P_{0+500} on either side emerges regardless of size fraction (Figures 2a and 2b) or whether we are plotting the raw or fitted POC data (Figures 2 and 4). This pattern suggests the following two regime pattern: an ascending regime that covers low to moderate P_0, where P_0 and P_{0+500} increase concurrently and maintain constant mesopelagic transfer efficiency ($TE_{P0+500} \sim 30\%$) (A to B in Figure 5a); a maximum in biological pump strength and efficiency at moderate P_0 (B in Figure 5a); and finally, a descending regime that covers moderate to high P_0, where P_{0+500} and TE_{P0+500} decrease with increasing P_0 (B to C in Figure 5a).

[38] The range in P_0 in this data set is defined by both spatial and temporal gradients in near-surface POC. Examining subsets of data collected during single cruises that span spatial gradients in P_0 best illustrates these two regimes. The two JGOFS Equatorial Pacific surveys covered a spatial gradient in productivity, biomass, and P_0 from 12°N to 12°S along 140°W, with EqPac1 (Figure 5b) sampled during a strong El Niño in 1992, and EqPac2 (Figure 5c) sampled six months later in "normal" conditions, when productivity was about twice as high [*Barber et al.*, 1996]. Both of these data subsets suggest a concurrent increase in P_0 and P_{0+500} along a contour of constant transfer efficiency at low to moderate

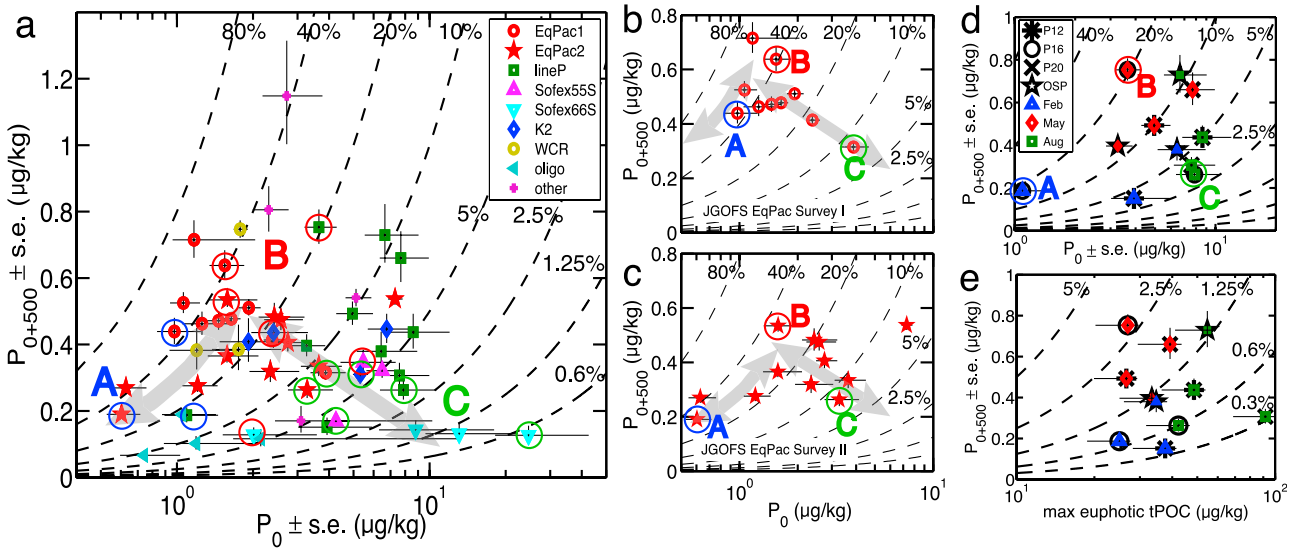

Figure 5. The dynamic nature of the biological pump. (a) Same as Figure 4a, but annotated to show movement within each regime (gray arrows) defined by the three vertices (A, B, C) as explained in section 3.4. (b–d) Subsets of the data plotted in Figure 5a, illustrating similar trends: JGOFS EqPac Survey I (Figure 5b), JGOFS EqPac Survey II (Figure 5c), and CJGOFS Line P (Figure 5d). (e) Same as Figure 5d, but plotted against the maximum total POC in the euphotic zone. Symbols for Figures 5b–5c as in Figure 5a. Symbols for Figures 5d–5e (Line P): Station locations are indicated by black symbols; time of sampling is overlaid in colored symbols. Ocean Station Papa (OSP) stations do not follow the general seasonal trend (see section 3.4) and are plotted in smaller symbols. Error bars and dashed contour lines as in Figure 4a. Full profiles for circled stations are plotted in Figure 6.

P_0, and decreasing P_{0+500} and TE_{P0+500} from moderate to high P_0.

[39] There appears to be no well-defined absolute value of P_0 that marks the boundary (vertex "B") between the ascending and descending regimes that is consistent between the two surveys, with the EqPac2 stations generally shifted to higher P_0, lower P_{0+500}, and lower mesopelagic transfer efficiency (Figures 5b and 5c). Although the same stations were occupied between the two surveys, there were significantly more eukaryotic phytoplankton during EqPac2 compared to the El Niño conditions of EqPac1 [*Bidigare and Ondrusek*, 1996].

[40] The data set also provides some examples of temporal changes in euphotic zone biomass and P_0, both over a seasonal time scale (the Line P stations) and also spanning the initiation or decline of several blooms (e.g., SOFeX, K2). As we will show in several case studies, we posit that high productivity bloom events plot in the descending regime (B to C in Figure 5a) and are characterized by decreasing mesopelagic transfer efficiency, with the height of the bloom defining the C vertex with lowest transfer efficiency. This decrease in transfer efficiency during bloom heights is generally due to concurrent increases in surface or near-surface POC (*maxPOC* or P_0) and decreases in deep mesopelagic POC (P_{500} or P_{0+500}).

[41] The first case study is the Line P stations in the eastern subarctic Pacific, which were sampled across a coastal to open ocean transect ("line P") over a seasonal cycle (Feb, May, August), combining spatial and temporal gradients in productivity [*Bishop et al.*, 1999]. The temporal change at any one station was generally greater than the spatial change across the line P transect; note for example the seasonal P16 data points highlighted by the "A," "B," and "C" labels (Figure 5d). Although the ascending and descending regimes are not as obvious in this data subset, there are some similar behaviors. The deep mesopelagic POC concentrations for stations P12, P16, and P20 cluster by season, with the lowest P_{0+500} in winter in February and the highest P_{0+500} in spring in May (Figure 5d). In August, they had the highest P_0 and euphotic zone total POC (*maxtPOC*), but lower deep mesopelagic POC (P_{0+500}) and transfer efficiency compared to May (Figures 5d–5e). These three stations (P12, P16, and P20) thus had the strongest and most efficient times of POC transfer in May, when biomass was moderately high but not blooming, but weak and inefficient POC transfer in August, when biomass was highest. The May to August behaviors are consistent with the descending regime trend to lower deep mesopelagic POC and lower transfer efficiency with increasing P_0 as seen in the global and EqPac data sets.

[42] A notable and interesting exception to this general seasonal grouping in the line P stations is at Ocean Station Papa (OSP), where the February OSP station plots with the other August stations, and the August OSP station plots with the other May stations (Figure 5d). Whereas the other stations along the line P transect are generally limited by major nutrients and exhibit a typical seasonal cycle, OSP is iron limited and has low seasonality [*Boyd and Harrison*, 1999; *Harrison*, 2002]. We hypothesize that iron limitation kept productivity at OSP in check in August 1996, keeping it from entering the descending regime and giving it characteristics more typical of May profiles at the other line P stations. In contrast, at the time of sampling at OSP in February 1996, there was an influx of iron from deep winter

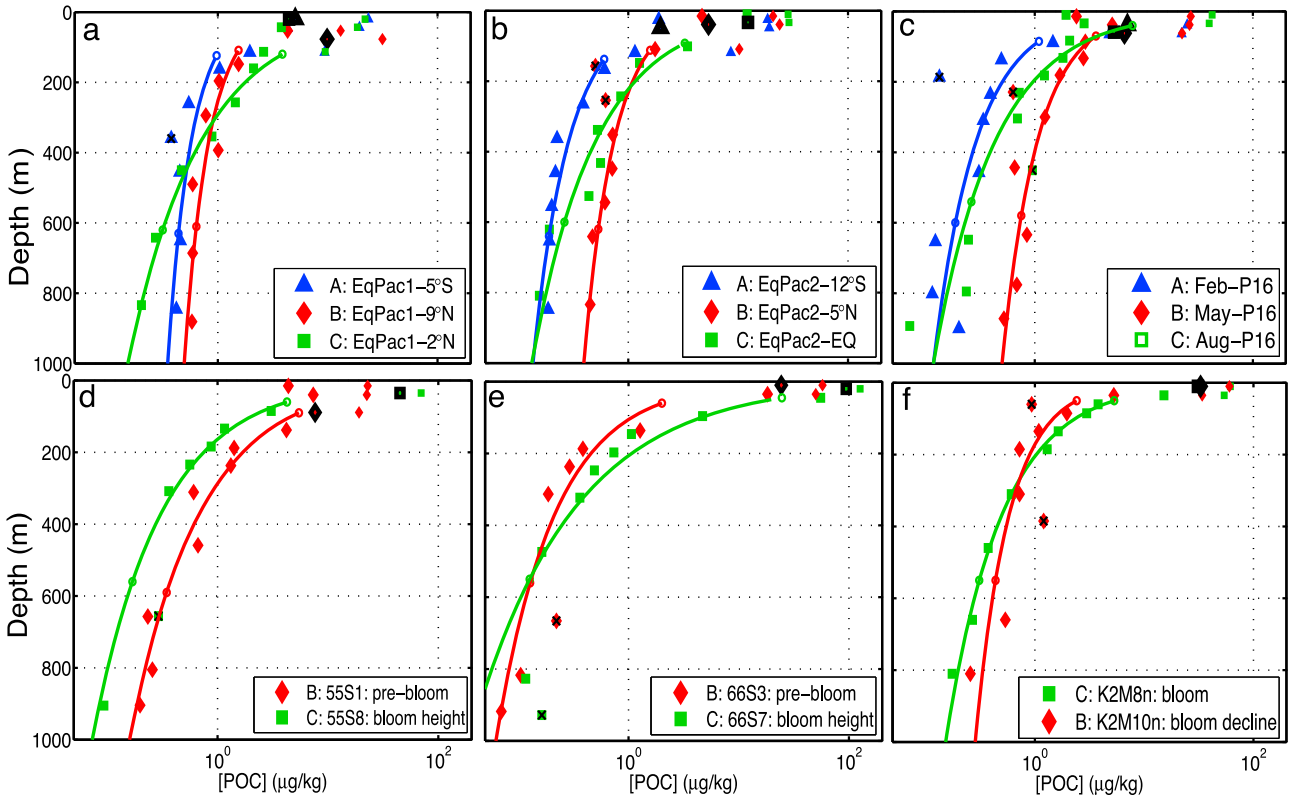

Figure 6. The >53 μm POC (solid symbols) profiles with power law fits (solid lines) and fitted P_0 and P_{0+500} (open circles) illustrating (a–c) typical profile shape in each of the three vertex regions, (d–e) during bloom initiation, or (f) during bloom decline. Maximum >53 μm euphotic POC outlined in black; euphotic zone total POC in small open symbols; symbols overlaid with black x not used in power law fit. Profiles plotting in the A, B, and C vertex regions are plotted in blue triangles, red diamonds, and green squares, respectively. All regions show an increase in attenuation of POC when P_0 is high or during blooming high biomass conditions (green). Profiles are from EqPac1 (Figure 6a), EqPac2 (Figure 6b), Station P16 (Line P) (Figure 6c), SOFeX 55°S (Figure 6d), SOFeX 66°S (Figure 6e), and Station K2 (western subarctic Pacific) (Figure 6f).

mixing that resulted in an unusual wintertime bloom [*Lam et al.*, 2006], which may have nudged it into the descending regime. Indeed, the contribution of large phytoplankton to total POC in the euphotic zone at OSP was greater in February (f_{large} = 0.41) than in August (f_{large} = 0.23), consistent with iron-stimulated production in February but not August. While OSP does not group by season with the other line P stations, it does group with the other stations if the groupings are defined by bloom state.

[43] Example profiles from the three vertex regions from the two EqPac surveys and station P16 from line P show the evolution of profile shape through the two regimes (Figures 6a–6c). The "A" type profile has the lowest P_0 and P_{0+500}. The "B" type profile has greater P_0 and P_{0+500}, maintaining a similar POC profile shape and thus mesopelagic transfer efficiency. The "C" type profile has a concurrent increase in P_0 and decrease in P_{0+500} compared to the "B" profile, and thus has the lowest mesopelagic transfer efficiency.

[44] None of the other projects in the data set had a sufficient number of profiles that covered a wide enough gradient in P_0 to look for ascending and descending regimes in P_0 versus P_{0+500} space, but individual profiles taken over time show the decrease in transfer efficiency with increasing surface or near-surface POC. In the second case study, MULVFS profiles taken over the course of the initiation of an artificially iron-induced bloom during the Southern Ocean Iron Experiment (SOFeX) in the Subantarctic (SOFeX 55°S) also show a clear decrease in deep mesopelagic POC 28 days after iron addition despite a more than sixfold increase in euphotic zone >53 μm POC, resulting in a factor of 13 reduction in the transfer efficiency of euphotic zone POC to 500 m, from 6% to 0.4% (Figure 6d). POC time series from an autonomous profiling float deployed at the start of the experiment confirm the maintenance of a low transfer efficiency condition throughout the bloom [*Bishop et al.*, 2004]. The bloom terminated with a subduction event several days after the last MULVFS profile at 55°S, and a ~10-day-long transient transfer of POC to depth followed before returning to near prebloom conditions [*Bishop et al.*, 2004]. Iron stimulation in the Antarctic (SOFeX 66°S) also resulted in a decrease in transfer efficiency 11 days after iron addition. This decrease was driven by increases in surface and near-surface POC, since P_{500} and P_{0+500} did not change (Figure 6e). We hypothesize that the decrease in deep mesopelagic POC after iron fertilization at 55°S but not at

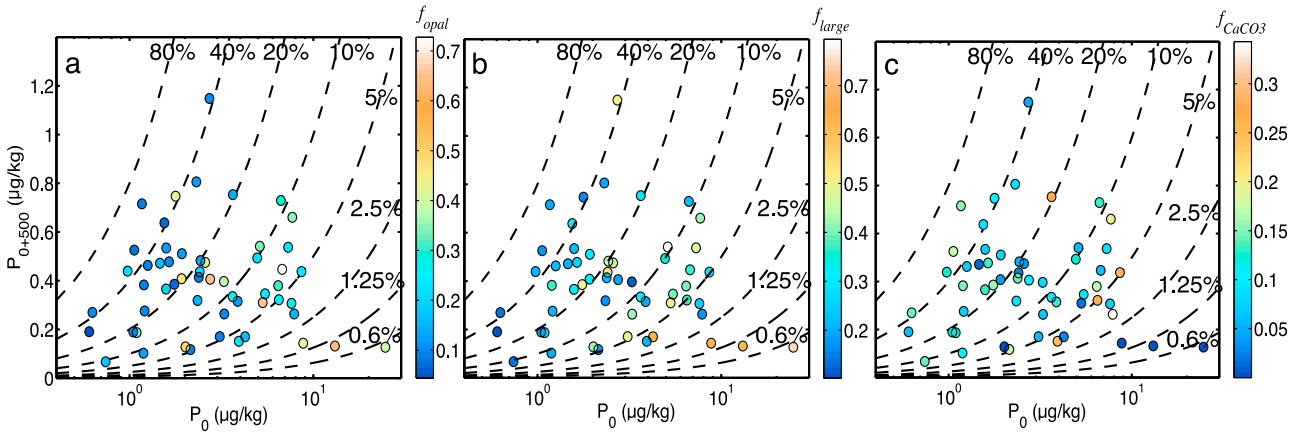

Figure 7. The fractional composition (by weight) at the depth of maximum >53 μm POC concentration in the euphotic zone for (a) opal (f_{opal} = $opal_{>53\mu m}$/$total\ mass_{>53\mu m}$, (b) large POC (f_{large} = $POC_{>53\mu m}$/POC_{total}), and (c) $CaCO_3$ (f_{CaCO3} = $CaCO3_{>53\mu m}$/$total\ mass_{>53\mu m}$), plotted in P_0-P_{0+500} space. Color bars show weight fractions between 0 and 1. Faint gray arrows indicate ascending and descending regimes described in section 3.4.

66°S was because iron addition dramatically altered community structure at 55°S but not at 66°S [*Lance et al.*, 2007].

[45] The data set also provides some insight into bloom termination for the third case study. Two day/night pairs of MULVFS profiles were taken over the course of a bloom decline at station K2 in the western subarctic Pacific from the VERTIGO project, suggesting a possible movement from C to B as a bloom terminates. Profiles 36–37 (K2M7d, K2M8n) were taken toward the end of a diatom bloom, and profiles 38–39 (K2M9d, K2M10n) were taken ~10 days later, several days after the termination of the bloom as evidenced by the twofold drop in chlorophyll and transmissometer-based POC concentrations in the euphotic zone [*Bishop and Wood*, 2008; *Buesseler et al.*, 2008]. P_0 dropped more than twofold between the two sets of profiles, while P_{0+500} remained the same or increased slightly, increasing the mesopelagic transfer efficiency from 6 to 7% during the bloom to 18–21% after the bloom (Figure 6f). Since the post bloom profiles were taken ~3 days after surface POC concentrations decreased [*Bishop and Wood*, 2008], and 50% of particles sank slower than 100 m/d [*Trull et al.*, 2008], it is possible that the mesopelagic stocks of POC had not yet fully adjusted to the lower surface concentrations above and that the mesopelagic transfer efficiency had not yet reached its maximum.

[46] Of the 10 artificial iron addition experiments to high nutrient, low chlorophyll waters that stimulated blooms, 5 showed no increase in shallow particle export flux during the course of the experiment, [*Boyd et al.*, 2007], pointing to low shallow export efficiency during a several weeks long bloom period. Our bloom case studies of >53 μm POC concentration profiles suggest that the bloom period itself can also be an extended time of low transfer efficiency in the mesopelagic, and that there is a period of order 1–2 weeks following the end of the bloom when the transfer efficiency may increase to a transient maximum during a sedimentation event before settling to a steady state intermediate efficiency.

3.5. Controls on Mesopelagic Transfer Efficiency: Community Structure

[47] While the data defining these trends are sometimes sparse, and there are certainly stations that do not follow the trends just described, the ascending and descending regimes linking near surface and deep mesopelagic POC provide a framework for understanding the factors that may govern a station's placement in P_0 and P_{0+500} space.

[48] We hypothesize that mesopelagic transfer efficiency is determined by the community composition of producers and consumers in the euphotic and mesopelagic zones. This notion finds support in long-term observations at the Bermuda Atlantic Time Series, where a shift in the phytoplankton community composition beginning in 1996 due to a shift in the phase of the North Atlantic Oscillation was associated with a decrease in mesopelagic transfer efficiency, defined as the flux at 300 m divided by the flux at 150 m [*Lomas et al.*, 2010]. The shift in community structure to a more eukaryotic-rich community between EqPac Surveys 1 and 2 was associated with a shift to lower transfer efficiencies, also consistent with the hypothesis that community structure determines transfer efficiencies.

[49] We speculate that the following mechanisms cause the dynamic change in the strength and efficiency of the biological pump. Profiles plotting near vertex A are winter or oligotrophic profiles. From A to B (the ascending regime), there is a gradual increase in productivity and biomass as light or nutrient limitation is gradually relieved. In the ascending regime, the strength of the biological pump scales with surface production, resulting in constant and high mesopelagic transfer efficiency because the euphotic and mesopelagic consumer communities are able to keep up with the gradually increasing producer community, packaging typically buoyant phytoplankton into fecal matter that can sink into the mesopelagic. From B to C (the descending regime), we enter the bloom mode: a particular environmental threshold is passed, allowing blooming organisms to prosper. Two potential mechanisms could explain the concurrent observed increase in shallow POC concentrations

Table 2. Regression Results From Single and Multiple Linear Regressions Between POC and $CaCO_3$ and Opal Concentrations in Upper 1000 m

		Single Linear Regressions								Multiple Linear Regressions				
		$CaCO_3$				Opal								
Depth Range (m)	Number of Observations	Slope	Intercept	R^2	p	Slope	Intercept	R^2	p	$CaCO_3$ Slope	Opal Slope	Intercept	R^2	p
0–115	165	1.15	3.66	0.18	<0.001	0.21	4.83	0.27	<0.001	0.73	0.17	3.35	0.33	<0.001
115–265	101	0.44	0.89	0.24	<0.001	0.08	1.10	0.08	0.003	0.41	0.06	0.79	0.28	<0.001
265–590	112	0.36	0.49	0.11	<0.001	0.04	0.60	0.04	0.033	0.34	0.03	0.47	0.13	<0.001
590–1000	96	0.43	0.24	0.08	0.005	0.01	0.35	0.00	0.756	0.46	−0.02	0.24	0.09	0.016

(*maxPOC* and P_0) with decrease in mesopelagic POC (P_{0+500}). In the first, the blooming producer community outpaces the ability of the euphotic zone consumer community to keep up with the sudden change in the type and amount of food. The decoupling between producers and consumers manifests as a loss of the particle repackaging function, and leads to an accumulation of biomass in the euphotic zone and reduction of particles exported to the mesopelagic. In the second mechanism, we posit that a blooming producer community is more labile than the diverse community it replaces, and is thus remineralized more efficiently in the upper mesopelagic, leading to low POC export to the deep mesopelagic. Both scenarios result in the observed increase in euphotic zone and reference depth POC concentrations (*maxPOC* and P_0) concurrent with a decrease in P_{0+500} as the mesopelagic is starved of its particle source. As a bloom terminates, it experiences a transient increase in TE_{P0+500} as surface particles sink, moving back from C toward B. Finally, we posit that the end of the growing season is marked by a gradual decrease in P_0 and P_{0+500}, plotting from B back to A.

3.6. Biogenic Ballast Minerals

[50] The MULVFS data set provides a crude indication about producer community composition through size fractionated (>53 μm versus <53 μm) POC and through the >53 μm opal and $CaCO_3$ concentrations that indicate the importance of siliceous and carbonate producing organisms. We use this information to examine the link between surface community composition and mesopelagic transfer efficiency as hypothesized above, and also to examine the importance of biogenic ballast minerals in determining the strength and efficiency of the biological pump.

[51] When the fractional composition of particles from the euphotic zone are plotted in P_0—P_{0+500} space, regions with the highest opal fractions ($f_{opal} > 0.3$) and a greater predominance of POC in the large size fraction ($f_{large} > 0.4$) tend to plot in the descending regime along the B—C trend (Figure 7), consistent with a community dominated by large diatoms and supporting the notion posed above that the descending regime is the blooming regime.

[52] In contrast, the ascending regime is characterized by relatively low opal fractions ($f_{opal} < 0.2$), a minor contribution of large particles ($f_{large} < 0.3$), and moderately high and relatively consistent $CaCO_3$ fraction ($f_{CaCO3} = 0.1–0.2$) (Figure 7). This is consistent with the notion of a relatively constant community structure throughout the ascending regime.

[53] Since diatom blooms plot in the descending regime, which is the most dynamic and variable part of the biological pump, spanning a range of P_{0+500} and crossing many contours of transfer efficiency (Figure 7a), it is not surprising that opal is a poor predictor for the strength or efficiency of the biological pump [*François et al.*, 2002; *Klaas and Archer*, 2002]. Some of the line P stations that plot in the descending regime also have relatively high f_{CaCO3} and should thus be expected to lower the predictive power of $CaCO_3$ for the biological pump. Nonetheless, the relative constancy of f_{CaCO3} through the ascending regime suggests that $CaCO_3$ should scale with both P_0 and P_{0+500} within this regime. This is consistent with both shallow and deep flux observations showing better correlations between POC flux with $CaCO_3$ flux compared to opal flux [*François et al.*, 2002; *Klaas and Archer*, 2002; *Sanders et al.*, 2010].

[54] In addition to using ballast minerals as indicators of surface community composition, we examined the relationship between POC and biogenic ballast mineral concentrations throughout the upper 1000 m. We binned the >53 μm particulate data into four depth zones (euphotic zone: 0–115 m; upper mesopelagic: 115–265 m; mid-mesopelagic: 265–590 m; lower mesopelagic: 590–1000 m) so that linear regressions of POC against $CaCO_3$ and opal could be performed. As expected from the analysis of euphotic zone ballast minerals above, there is a better correlation between POC and $CaCO_3$ concentrations at all depth bins in the mesopelagic than with opal (Table 2), although even the $CaCO_3$ correlations were far weaker ($R^2 < 0.25$) than observed for either deep or shallow flux data. *Sanders et al.* [2010] observed generally higher relative biomineral compositions in exported material compared to >0.2 μm suspended particles, and interpreted this to support the mechanistic role for ballast minerals in promoting faster sinking.

[55] Alternatively, we can view biogenic ballast minerals not as direct agents for the enhancement of particle sinking, but rather as imperfect proxies for ecosystem structure. Given the lack of a consistent relationship between POC flux and ballast mineral flux in a time series setting at OSP [*Wong et al.*, 1999] or at Bermuda [*Conte et al.*, 2001], the case for a direct role for ballast minerals in promoting POC flux is still equivocal [*Boyd and Trull*, 2007]. Rather, our analysis of the dynamic biological pump suggests that $CaCO_3$ producers are an integral part of the type of ecosystems that promote high transfer efficiencies and high P_{0+500} at moderate P_0. As others have hypothesized before [*François et al.*, 2002], carbonate producing ecosystems may be more complex, and thus the particles have been

reworked more thoroughly before escaping the euphotic zone, and are thus transferred more efficiently through the mesopelagic.

3.7. Consistency Between >53 μm POC Concentration and POC Flux Profiles

[56] Can the trends that we see in the analysis of POC concentration profiles be applied to POC flux profiles? Two stations in the data set (profiles 5–6 in the Panama Basin and 36–39 at Station K2 in the western subarctic Pacific) had complementary mesopelagic flux estimates that enabled evaluation of the analysis of >53 μm POC profiles as a meaningful complement to POC flux data. Both stations had POC flux and >53 μm POC profile observations over at least 2 deployments that showed a similar dramatic change in the magnitude and shape of POC concentration and flux between deployments. The Panama Basin fluxes were calculated from empirically determined settling velocity relationships for size and shape-classified fecal matter [*Bishop et al.*, 1986] and fit as described above, and the K2 fluxes were measured using a variety of surface tethered and neutrally buoyant sediment traps [*Lamborg et al.*, 2008] and fit as described by *Buesseler and Boyd* [2009]. Power law fit parameters to the POC flux data show consistent temporal trends as those from >53 μm POC concentration data between deployments (Figure S2), with the b value increasing at the Panama Basin and decreasing at Station K2 between the two deployments, and P_0 decreasing between the two deployments at both stations.

[57] Based on the consistent temporal trends between the concentration and flux at these two sites, we hypothesize that the geographical and temporal trends from the analysis of POC concentration profiles may also be indicative of the patterns in POC flux profiles.

3.8. Toward a Climatology of the Biological Pump

[58] We have shown that the biological pump is extremely dynamic, with a station in the subarctic Pacific capable of spanning almost the entire global range of strength and efficiency over a seasonal cycle (Figure 5a). It is likely that lower latitude stations would have less of a temporal dynamic range. It is also plausible that different regions would spend different lengths of time in each regime. Indeed, the annual average strength and efficiency of the biological pump is likely to vary from region to region, and will be a function of the dynamic range experienced by that station, and how long a station spends in each regime. The fate of POC in each regime will depend on the factors governing the maintenance and termination of the bloom at that location, and is probably difficult to predict. Since the initiation, height, and decline of a bloom cross so many contours of transfer efficiency, we cannot say what the net pump strength and efficiency are over the course of a bloom. Even within the realm of the better studied shallow export, examples abound in the literature of the entire range of behavior of bloom fate, from blooms that never export [e.g., *Kiørboe et al.*, 1996], to blooms in which there is a rapid massive sedimentation of phytoplankton aggregates [e.g., *Alldredge et al.*, 1995], and everything in between. There will surely also be a range in the fate of POC in the mesopelagic that may not fit our two regime conceptual view. Nonetheless, this global POC data set suggests a framework for thinking about the strength and efficiency of the biological pump in the mesopelagic, and points to the critical need for time series measurements in different biogeographic regions to build a climatological view of the strength and efficiency of the biological pump.

[59] Various strategies have recently been employed to greatly increase the temporal and spatial data coverage of POC concentration in the mesopelagic, including the use of ship-deployed particle imaging systems [*Guidi et al.*, 2009, 2007; *McDonnell et al.*, 2009] and autonomous profiling floats and gliders with optical sensors [*Bishop and Wood*, 2009; *Boss et al.*, 2008; *Johnson et al.*, 2009]. While these new optical techniques do not have the advantage that physical samples have for complementary additional geochemical analyses, their unparalleled ability to obtain high depth and time resolution profiles will certainly improve our data coverage in the future.

4. Conclusions

[60] We find large geographic and temporal variability in the mesopelagic transfer efficiency (attenuation length scale) of POC using a global data set of >53 μm POC concentrations in the upper 1000 m. We show that the strength and efficiency of the biological pump are dynamic and are characterized by two regimes: (1) a constant and high mesopelagic transfer efficiency regime at low to moderate P_0 and (2) a bloom regime in which the height of the bloom is characterized by a weak deep biological pump and low transfer efficiency.

[61] The variability in attenuation length scale of POC manifests in a clear decoupling between the strength of the shallow pump (P_0) and the strength of the deep pump (P_{0+500}). We suggest that the paradigm of diatom-driven export production is driven by a too restrictive perspective on upper mesopelagic dynamics. Indeed, our full mesopelagic analysis suggests that large, blooming diatoms have low transfer efficiency and thus may not export substantially to depth. Rather, ecosystems characterized by smaller cells and moderately high $\%CaCO_3$ have a high mesopelagic transfer efficiency and can have higher POC concentrations in the deep mesopelagic even with relatively low surface or near-surface POC. This has negative implications for the carbon sequestration prospects of deliberate iron fertilization, which typically shifts community composition from a more complex and diverse mix of organisms with high mesopelagic transfer efficiency to a diatom-dominated assemblage with low transfer efficiency.

[62] Time series studies of euphotic and mesopelagic POC concentration and flux in a variety of biogeographic regions are desperately needed to determine how long a region spends in each regime. These POC measurements need to be paired with euphotic and mesopelagic community structure determinations to enable predictive modeling of POC attenuation as a function of changing community structure. This will not only improve understanding of how the current system works, but allow projections into the future under a changing climate. Recent modeling studies have shown that ocean CO_2 storage is sensitive to the attenuation length scale of POC [*Kwon et al.*, 2009; *Matsumoto*, 2007]. We suggest

that global biogeochemical models need to vary the attenuation length scale (b value) in both time and space based on community composition.

[63] **Acknowledgments.** This manuscript has benefited from helpful discussions with Carl Lamborg, Andrew Solow, and Ken Buesseler and comments from two anonymous reviewers. Funding for P.J.L. for this synthesis was from the WHOI Ocean and Climate Change Institute. S.C.D. was supported by the WHOI W. Van Alan Clark Senior Chair.

References

Alldredge, A. L., et al. (1995), Mass aggregation of diatom blooms: Insights from a mesocosm study, *Deep Sea Res., Part II*, *42*, 9–27, doi:10.1016/0967-0645(95)00002-8.

Anderson, L. A. (1995), On the hydrogen and oxygen content of marine phytoplankton, *Deep Sea Res., Part I*, *42*, 1675–1680, doi:10.1016/0967-0637(95)00072-E.

Anderson, L. A., and J. L. Sarmiento (1994), Redfield ratios of remineralization determined by nutrient data analysis, *Global Biogeochem. Cycles*, *8*, 65–80, doi:10.1029/93GB03318.

Armstrong, R. A., et al. (2002), A new, mechanistic model for organic carbon fluxes in the ocean based on the quantitative association of POC with ballast minerals, *Deep Sea Res., Part II*, *49*, 219–236, doi:10.1016/S0967-0645(01)00101-1.

Barber, R. T., et al. (1996), Primary productivity and its regulation in the equatorial Pacific during and following the 1991–1992 El Niño, *Deep Sea Res., Part II*, *43*, 933–969, doi:10.1016/0967-0645(96)00035-5.

Berelson, W. M. (2001), The flux of particulate organic carbon into the ocean interior: A comparison of four U.S. JGOFS regional studies, *Oceanography*, *14*, 59–67.

Bidigare, R. R., and M. E. Ondrusek (1996), Spatial and temporal variability of phytoplankton pigment distributions in the central equatorial Pacific Ocean, *Deep Sea Res., Part II*, *43*, 809–833, doi:10.1016/0967-0645(96)00019-7.

Bishop, J. K. B. (1992), POC from MULVFS casts, 25 September 2002, accessed 6 February 2010, http://usjgofs.whoi.edu/jg/serv/jgofs/eqpac/tt007/mulvfs_POC.html0, U.S. JGOFS Data Server, U.S. JGOFS Data Manage. Off. WHOI, Woods Hole, Mass.

Bishop, J. K. B. (1999), Transmissometer measurement of POC, *Deep Sea Res., Part I*, *46*, 353–369, doi:10.1016/S0967-0637(98)00069-7.

Bishop, J. K. B., and M. Q. Fleisher (1987), Particulate manganese dynamics in gulf-stream warm-core rings and surrounding waters of the NW Atlantic, *Geochim. Cosmochim. Acta*, *51*, 2807–2825, doi:10.1016/0016-7037(87)90160-8.

Bishop, J. K. B., and T. J. Wood (2008), Particulate matter chemistry and dynamics in the twilight zone at VERTIGO ALOHA and K2 sites, *Deep Sea Res., Part I*, *55*, 1684–1706, doi:10.1016/j.dsr.2008.07.012.

Bishop, J. K. B., and T. J. Wood (2009), Year-round observations of carbon biomass and flux variability in the Southern Ocean, *Global Biogeochem. Cycles*, *23*, GB2019, doi:10.1029/2008GB003206.

Bishop, J. K. B., et al. (1977), Chemistry, biology, and vertical flux of particulate matter from upper 400 m of equatorial Atlantic Ocean, *Deep Sea Res.*, *24*, 511–548, doi:10.1016/0146-6291(77)90526-4.

Bishop, J. K. B., et al. (1978), Chemistry, biology and vertical flux of particulate matter from the upper 400 m of the Cape Basin in the southeast Atlantic Ocean, *Deep Sea Res.*, *25*, 1121–1161, doi:10.1016/0146-6291(78)90010-3.

Bishop, J. K. B., et al. (1980), The chemistry, biology, and vertical flux of particulate matter from the upper 1500 m of the Panama Basin, *Deep Sea Res., Part A*, *27*, 615–640.

Bishop, J. K. B., et al. (1985), A multiple-unit large-volume in-situ filtration system for sampling oceanic particulate matter in mesoscale environments, in *Mapping Strategies in Chemical Oceanography*, *Adv. Chem.*, vol. 209, chap. 9, pp. 155–175, Am. Chem. Soc., Washington, D. C., doi:10.1021/ba-1985-0209.ch009.

Bishop, J. K. B., et al. (1986), Particulate matter distributions, chemistry and flux in the Panama Basin: Response to environmental forcing, *Prog. Oceanogr.*, *17*, 1–59, doi:10.1016/0079-6611(86)90024-8.

Bishop, J. K. B., et al. (1999), Spatial and temporal variability of POC in the northeast subarctic Pacific, *Deep Sea Res., Part II*, *46*, 2699–2733, doi:10.1016/S0967-0645(99)00081-8.

Bishop, J. K. B., et al. (2004), Robotic observations of enhanced carbon biomass and export at 55 degrees S during SOFeX, *Science*, *304*, 417–420, doi:10.1126/science.1087717.

Boss, E., et al. (2008), Observations of pigment and particle distributions in the western North Atlantic from an autonomous float and ocean color satellite, *Limnol. Oceanogr.*, *53*, 2112–2122, doi:10.4319/lo.2008.53.5_part_2.2112.

Boyd, P., and P. J. Harrison (1999), Phytoplankton dynamics in the NE subarctic Pacific, *Deep Sea Res., Part II*, *46*, 2405–2432, doi:10.1016/S0967-0645(99)00069-7.

Boyd, P. W., and T. W. Trull (2007), Understanding the export of biogenic particles in oceanic waters: Is there consensus?, *Prog. Oceanogr.*, *72*, 276–312, doi:10.1016/j.pocean.2006.10.007.

Boyd, P. W., et al. (2007), Mesoscale iron enrichment experiments 1993–2005: Synthesis and future directions, *Science*, *315*, 612–617, doi:10.1126/science.1131669.

Buesseler, K. O. (1998), The decoupling of production and particulate export in the surface ocean, *Global Biogeochem. Cycles*, *12*, 297–310, doi:10.1029/97GB03366.

Buesseler, K. O., and P. W. Boyd (2009), Shedding light on processes that control particle export and flux attenuation in the twilight zone of the open ocean, *Limnol. Oceanogr.*, *54*, 1210–1232, doi:10.4319/lo.2009.54.4.1210.

Buesseler, K. O., et al. (2007a), An assessment of the use of sediment traps for estimating upper ocean particle fluxes, *J. Mar. Res.*, *65*, 345–416.

Buesseler, K. O., et al. (2007b), Revisiting carbon flux through the ocean's twilight zone, *Science*, *316*, 567–570, doi:10.1126/science.1137959.

Buesseler, K. O., et al. (2008), VERTIGO (Vertical Transport in the Global Ocean): A study of particle sources and flux attenuation in the North Pacific, *Deep Sea Res., Part II*, *55*, 1522–1539, doi:10.1016/j.dsr2.2008.04.024.

Conte, M. H., et al. (2001), Seasonal and interannual variability in deep ocean particle fluxes at the Oceanic Flux Program (OFP)/Bermuda Atlantic Time Series (BATS) site in the western Sargasso Sea near Bermuda, *Deep Sea Res., Part II*, *48*, 1471–1505, doi:10.1016/S0967-0645(00)00150-8.

François, R., et al. (2002), Factors controlling the flux of organic carbon to the bathypelagic zone of the ocean, *Global Biogeochem. Cycles*, *16*(4), 1087, doi:10.1029/2001GB001722.

Guidi, L., et al. (2007), Vertical distribution of aggregates (>110 μm) and mesoscale activity in the northeastern Atlantic: Effects on the deep vertical export of surface carbon, *Limnol. Oceanogr.*, *52*, 7–18, doi:10.4319/lo.2007.52.1.0007.

Guidi, L., et al. (2008), Relationship between particle size distribution and flux in the mesopelagic zone, *Deep Sea Res., Part I*, *55*, 1364–1374, doi:10.1016/j.dsr.2008.05.014.

Guidi, L., et al. (2009), Effects of phytoplankton community on production, size and export of large aggregates: A world-ocean analysis, *Limnol. Oceanogr.*, *54*, 1951–1963, doi:10.4319/lo.2009.54.6.1951.

Harrison, P. J. (2002), Station Papa time series: Insights into ecosystem dynamics, *J. Oceanogr.*, *58*, 259–264, doi:10.1023/A:1015857624562.

Hedges, J. I., et al. (2002), The biochemical and elemental compositions of marine plankton: A NMR perspective, *Mar. Chem.*, *78*, 47–63, doi:10.1016/S0304-4203(02)00009-9.

Honjo, S., et al. (2008), Particulate organic carbon fluxes to the ocean interior and factors controlling the biological pump: A synthesis of global sediment trap programs since 1983, *Prog. Oceanogr.*, *76*, 217–285, doi:10.1016/j.pocean.2007.11.003.

Johnson, K. S., et al. (2009), Observing biogeochemical cycles at global scales with profiling floats and gliders: Prospects for a global array, *Oceanography*, *22*, 216–225.

Kiørboe, T., et al. (1996), Sedimentation of phytoplankton during a diatom bloom: Rates and mechanisms, *J. Mar. Res.*, *54*, 1123–1148, doi:10.1357/0022240963213754.

Klaas, C., and D. E. Archer (2002), Association of sinking organic matter with various types of mineral ballast in the deep sea: Implications for the rain ratio, *Global Biogeochem. Cycles*, *16*(4), 1116, doi:10.1029/2001GB001765.

Kwon, E. Y., et al. (2009), The impact of remineralization depth on the air-sea carbon balance, *Nat. Geosci.*, *2*, 630–635, doi:10.1038/ngeo612.

Lam, P. J., and J. K. B. Bishop (2007), High biomass low export regimes in the Southern Ocean, *Deep Sea Res., Part II*, *54*, 601–638, doi:10.1016/j.dsr2.2007.01.013.

Lam, P. J., et al. (2006), Wintertime phytoplankton bloom in the subarctic Pacific supported by continental margin iron, *Global Biogeochem. Cycles*, *20*, GB1006, doi:10.1029/2005GB002557.

Lamborg, C. H., et al. (2008), The flux of bio- and lithogenic material associated with sinking particles in the mesopelagic "twilight zone" of the northwest and north central Pacific Ocean, *Deep Sea Res., Part II*, *55*, 1540–1563, doi:10.1016/j.dsr2.2008.04.011.

Lance, V. P., et al. (2007), Primary productivity, differential size fraction and pigment composition responses in two Southern Ocean in situ iron enrichments, *Deep Sea Res., Part I*, *54*, 747–773, doi:10.1016/j.dsr.2007.02.008.

Lee, C., et al. (2009), Particulate organic matter and ballast fluxes measured using time-series and settling velocity sediment traps in the northwestern Mediterranean Sea, *Deep Sea Res., Part II*, *56*, 1420–1436, doi:10.1016/j.dsr2.2008.11.029.

Lee, Z., et al. (2007), Euphotic zone depth: Its derivation and implication to ocean-color remote sensing, *J. Geophys. Res.*, *112*, C03009, doi:10.1029/2006JC003802.

Lomas, M. W., et al. (2010), Increased ocean carbon export in the Sargasso Sea linked to climate variability is countered by its enhanced mesopelagic attenuation, *Biogeosciences*, *7*, 57–70, doi:10.5194/bg-7-57-2010.

Lutz, M., et al. (2002), Regional variability in the vertical flux of particulate organic carbon in the ocean interior, *Global Biogeochem. Cycles*, *16*(3), 1037, doi:10.1029/2000GB001383.

Marinov, I., et al. (2006), The Southern Ocean biogeochemical divide, *Nature*, *441*, 964–967, doi:10.1038/nature04883.

Martin, J. H., et al. (1987), Vertex: Carbon cycling in the northeast Pacific, *Deep Sea Res., Part A*, *34*, 267–285.

Matsumoto, K. (2007), Biology-mediated temperature control on atmospheric pCO_2 and ocean biogeochemistry, *Geophys. Res. Lett.*, *34*, L20605, doi:10.1029/2007GL031301.

Matsumoto, K., et al. (2007), Effect of temperature-dependent organic carbon decay on atmospheric pCO_2, *J. Geophys. Res.*, *112*, G02007, doi:10.1029/2006JG000187.

McDonnell, A. M. P., et al. (2009), Relating stocks and sinking fluxes of particles in the mesopelagic zone: Case studies from the west Antarctic peninsula and the subtropical North Atlantic, paper presented at AGU Chapman Conference on the Biological Carbon Pump of the Oceans, Natl. Oceanogr. Cent., Brockenhurst, U. K., 1–4 Sept.

Primeau, F. (2006), On the variability of the exponent in the power law depth dependence of POC flux estimated from sediment traps, *Deep Sea Res., Part I*, *53*, 1335–1343, doi:10.1016/j.dsr.2006.06.003.

Sanders, R., et al. (2010), Does a ballast effect occur in the surface ocean?, *Geophys. Res. Lett.*, *37*, L08602, doi:10.1029/2010GL042574.

Sherry, N. D., et al. (1999), Seasonal and spatial patterns of heterotrophic bacterial production, respiration, and biomass in the subarctic NE Pacific, *Deep Sea Res., Part II*, *46*, 2557–2578, doi:10.1016/S0967-0645(99)00076-4.

Smith, R. C., and K. S. Baker (1985), Spatial and temporal patterns in pigment biomass in Gulf Stream warm-core ring 82 B and its environs, *J. Geophys. Res.*, *90*, 8859–8870, doi:10.1029/JC090iC05p08859.

Stemmann, L., et al. (2004), A vertical model of particle size distributions and fluxes in the midwater column that includes biological and physical processes: Part I: Model formulation, *Deep Sea Res., Part I*, *51*, 865–884, doi:10.1016/j.dsr.2004.03.001.

Timothy, D. A., et al. (2003), Settling fluxes in Saanich and Jervis inlets, British Columbia, Canada: Sources and seasonal patterns, *Prog. Oceanogr.*, *59*, 31–73, doi:10.1016/j.pocean.2003.07.001.

Trees, C. C. (1992a), Bio-optical profiler data, 25 September 2002, accessed 6 February 2010, http://usjgofs.whoi.edu/jg/serv/jgofs/eqpac/tt007/optics, U.S. JGOFS Data Server, U.S. JGOFS Data Manage. Off., WHOI, Woods Hole, Mass.

Trees, C. C. (1992b), Bio-optical profiler data, 25 September 2002, accessed 6 February 2010, http://usjgofs.whoi.edu/jg/serv/jgofs/eqpac/tt011/optics, U.S. JGOFS Data Server, U.S. JGOFS Data Manage. Off., WHOI, Woods Hole, Mass.

Trull, T. W., et al. (2008), In situ measurement of mesopelagic particle sinking rates and the control of carbon transfer to the ocean interior during the Vertical Flux in the Global Ocean (VERTIGO) voyages in the North Pacific, *Deep Sea Res., Part II*, *55*, 1684–1695, doi:10.1016/j.dsr2.2008.04.021.

Volk, T., and M. I. Hoffert (1985), Ocean carbon pumps: Analysis of relative strengths and efficiencies in ocean-driven atmospheric CO_2 changes, in *The Carbon Cycle and Atmospheric CO_2 Natural Variations Archean to Present*, *Geophys. Monogr. Ser.*, vol. 32, edited by E. T. Sundquist and W. S. Broecker, pp. 99–110, AGU, Washington, D. C., doi:10.1021/ba-1985-0209.ch009. *Geophys. Monogr.*, *32*, 99–110.

Wong, C. S., et al. (1999), Seasonal and interannual variability in particle fluxes of carbon, nitrogen and silicon from time series of sediment traps at Ocean Station P, 1982–1993: Relationship to changes in subarctic primary productivity, *Deep Sea Res., Part II*, *46*, 2735–2760, doi:10.1016/S0967-0645(99)00082-X.

Yu, E. F., et al. (2001), Trapping efficiency of bottom-tethered sediment traps estimated from the intercepted fluxes of Th-230 and Pa-231, *Deep Sea Res., Part I*, *48*, 865–889, doi:10.1016/S0967-0637(00)00067-4.

J. K. B. Bishop, Department of Earth and Planetary Science, University of California, 307 McCone Hall, Berkeley, CA 94720, USA.

S. C. Doney and P. J. Lam, Department of Marine Chemistry and Geochemistry, Woods Hole Oceanographic Institution, M.S. 35, 360 Woods Hole Rd., Woods Hole, MA 02540, USA. (pjlam@whoi.edu)